LIGO SURF: Enhancement of Second Harmonic Generation for Squeezing in aLIGO

Nathan Z. Zhao, Columbia University
Mentors: Dick Gustafson and Daniel Sigg

September 1, 2014

Abstract

Second harmonic generation is employed to increase LIGO's sensitivity in the shot noise dominated bandwidth (100 Hz and above) by introducing squeezed states through the dark port of the interferometer. This project characterizes and improves the second harmonic generation of periodically poled KTP in a resonant cavity locked by a PDH servo. These enhancements include custom mechanical stages to control movement of the mirrors in the horizontal direction and retain information about optimal mirror positions if the mirror mounts need to be moved. Additionally, a digital temperature controller featuring Beckhoff Ethercat terminals and TwinCat PLC software. The servo's response characteristics (set-temperature response and step function response) have been analyzed and suggest stable performance on the order of days.

1 Introduction and Background

1.1 Squeezing in aLIGO

LIGO employs squeezing to improve interferometer sensitivity at shot noise limited frequencies (100 Hz and above) without increasing the beam power. Shot noise is optical intensity noise arising from the discreteness of light (or the electromagnetic field in general) at the quantum level. For example, it can be measured as random fluctuations in the number of photodetection

events from a constant intensity beam on a photodetector. Shot noise is governed by poisson's distribution:

$$p(n) = \frac{\mu^{-n} e^{-\mu}}{n!} \tag{1}$$

where μ is the mean of the system. Note that the distribution can be fairly well approximated by the normal distribution for high n (number of events).

Reducing shot noise is done by introducing squeezed states. Shot noise itself is a result of vacuum fluctuations of the electromagnetic field, but Heisenberg's Uncertainty principle limits the product of quadrature deviations of phase and amplitude of the E-complex field to some minimum value. Thus, one can reduce deviations in quadrature at the cost of increasing it in the other, a squeezed state.

1.2 Second Harmonic Generation

Squeezed states are achieved in LIGO via second harmonic generation. Second harmonic generation is a nonlinear optical effect whereby two photons of a fundamental frequency are combined to produce a photon at twice the fundamental frequency. [1] The phenomenon can be approached through its mathematical description. In the realm of linear optics, a dielectric's polarization is given by the relation: $\mathbf{P} = \epsilon_0 \chi^{(1)} \mathbf{E}$, where $\chi^{(1)}$ is the susceptibility of the material (this is a scalar for isotropic materials, a rank two tensor for anisotropic materials) This, however, is just an approximation, albeit a good one for most materials. For cases outside the linear realm, the real, nonlinear polarization (dipole per unit volume) is better approximated by a power series:

$$\mathbf{P} = \epsilon_0(\chi^{(1)}_{ij} E_i + \chi^{(2)}_{ijk} E_i E_j + \chi^{(3)}_{ijkl} E_i E_j E_k + ... \tag{2}$$

Second harmonic generation is a result of the second order term $\chi^{(2)}_{ijk} E_i E_j$. To understand how a frequency doubled photon emerges as a result of this term, consider the electric component of a propagating EM wave (i.e. a laser):

$$\mathbf{E}_i = \mathbf{E}_{0i} e^{-iwt} + c.c \tag{3}$$

[1] This by itself is not what produces a squeezed state. An optical parametric isolater is needed to

with the real part:

$$Re(\mathbf{E}_i) = \frac{1}{2}(\mathbf{E}_{0i}e^{-iwt} + \mathbf{E}^*_{0i}e^{iwt}) + c.c \tag{4}$$

If we place the real part of the electric field component into the second order contribution to the polarization, we get:

$$\chi^{(2)}_{ijk}(E^2_{0i}e^{-i2wt} + E^{*2}_{0i}e^{i2wt} + E_{0i}E^*_{0i}) + c.c \tag{5}$$

Equation 4 shows that the second order polarization has two contributions. The first is $E_{0i}E^*_{0i}$, which has no time dependence and produces no radiation. This term describes the production of a static electric field across the crystal (this is a separate phenomenon called optical rectification) [2]. The second contribution, occurring at a frequency of 2ω, is the characteristic SHG effect. Theoretically, the frequency doubling effect can be visualized with the destruction of two incident photons of frequency ω to produce one photon at frequency 2ω. Finally, note that second harmonic generation is just one phenomenon of frequency changes in non-linear materials. Sum-frequency, Difference-frequency generation, third harmonic generation are all similar effects arising with appreciable nonlinear susceptibility [2].

Another peculiar property of SHG is its exclusive characterization in non-centrosymmetric crystal geometries. This too is derivable from the second order term in the power series expansion of the polarization. A centrosymmetric media is invariant under the transformation $r \to -(r)$. If we flip the sign of the electric field, then the sign of first-order polarization ($\mathbf{P} = \epsilon_0\chi^{(1)}\mathbf{E}$) is also flipped. But a quadratic term stays positive under the sign change, meaning the second order term cannot switch signs with the transformation. Second harmonic generation is physically possible only if centrosymmetry is violated [6]; the lowest order non-linear effect in a centro-symmetric crystal is thus third-order, not second order.

1.3 Phase Matching

The production of frequency doubled light is naturally diminished by phase mismatch of the carrier beam and the green light. That is, if the phase and direction of the second harmonic light rays do not match (see figure 1) [2] with themselves and the fundamental, they will destructively interfere and attenuate the second harmonic effect.

[2]match means that the peaks and troughs of the IR and green light coincides

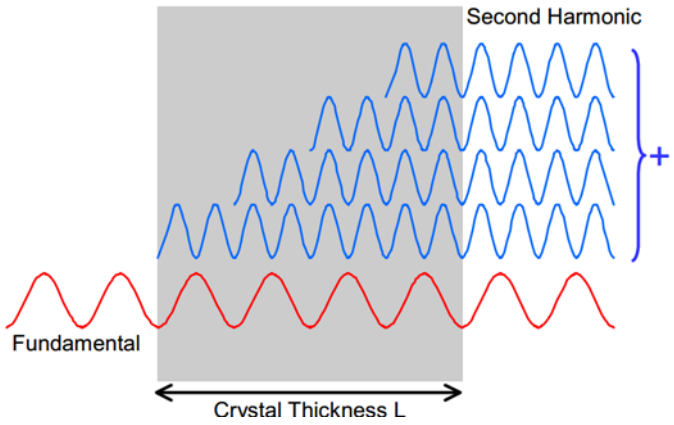

Figure 1: phase matching [4]

The mathematical starting point of phase matching is simply Maxwell's wave equation in a dielectric, *nonlinear* medium:

$$\nabla^2 \tilde{E}_n - \frac{\epsilon^{1()}\omega_n}{c^2}(\frac{\partial^2 \tilde{E}_n}{\partial t^2}) = (\frac{1}{\epsilon_0 c^2})\frac{\partial^2 \tilde{P}_n}{\partial t^2} \tag{6}$$

[2] The nonlinear equation must hold for the carrier wave and the second harmonic. Assuming the nonlinear source term is 0, then a plane wave $A_3 e^{i(k_3 z - \omega t)} + c.c$ where A_3 is constant satisfies the nonlinear wave equation. For a small nonlinear source term then, it would be reasonable to expect that A_3 would become a slowly varying function of z. This is enough to use it as a trial solution to the nonlinear equation with the source term. [2]

For simplification, we'll assume a simple source term given by:

$$P_3(\tilde{z}, t) = P_3 e^{-i\omega t} + c.c \tag{7}$$

with amplitude:

$$P_3 = 4\epsilon_0 d_{eff} E_1 E_2 \tag{8}$$

[2]

The electric field of the traveling EM wave propagating through the dielectric has the form:

$$\tilde{E}_i(z, t) = A_i e^{i(k_i z - \omega t)} + c.c \tag{9}$$

where A_i represents the amplitude of the wave.

The amplitude of the nonlinear polarization is now given by substituting E_1 and E_2:

$$P_3 = 4\epsilon_0 d_{eff} A_1 A_2 e^{i(k_1+k_2)z} \tag{10}$$

where $k_1 = k_2$ for SHG.

Combining all terms into the nonlinear wave equation and simplifying:

$$\frac{\partial^2 A_3}{\partial z^2} + 2ik_3 \frac{\partial A_3}{\partial z} = \frac{-4\epsilon_0 d_{eff} \omega_3^2}{c^2} A_1 A_2 e^{i(2k_1-k_3)z} \tag{11}$$

At this point, we can define the phase matching term $\Delta k = 2k_1 - k_3$. This term is called the wavevector mismatch [2]. Before this term is of any use, one approximation should be made to simplify the wave equation even further; the slowly varying amplitude approximation. [2], defined by:

$$|\frac{\partial^2 A_3}{\partial z^2}| << |k_3 \frac{\partial A_3}{\partial z}| \tag{12}$$

When this term is 0, then the amplitude of the second harmonic wave increases linearly with z, which implies the power scales quadratically with z. From the atomic point of view, $\Delta k = 0$ means that all the atomic dipoles emit light that is phased so that they add coherently in the forward direction. [2] If we further assume that the number of atoms is proportional to z, then we can also see that the power scales qudratically with the number of atomic dipoles as well.

If some phase mismatch occurs, we can integrate equation 14 and square it to approximate the intensity. [2]

$$I_3 = GL^2 sinc^2(\frac{\Delta kL}{2}) \tag{13}$$

where L is the length of the crystal. We can expect then the phase matching curve to look something like a sinc-squared function for various degrees of matching and with an obvious maximum when the mismatch is precisely 0. A more accurate expression of the algebraic constant is:

We can also express Δk in terms of the index of refraction for the carrier and the 2nd harmonic (recall that in a dielectric, the index of refraction is frequency dependent);

$$\Delta k(\lambda) = \frac{4\pi}{\lambda}(n(\lambda) - n(2\lambda)) \tag{14}$$

Equation 15 effectively says the problem of phase matching can be traced to getting the indices of refraction for the carrier and second harmonic to match. And this can be effectively done by changing the temperature of the crystal, which affects the indices of refraction. [11]

2 Experimental Methods

2.1 What is the SHG

2.2 The Optical Set-up

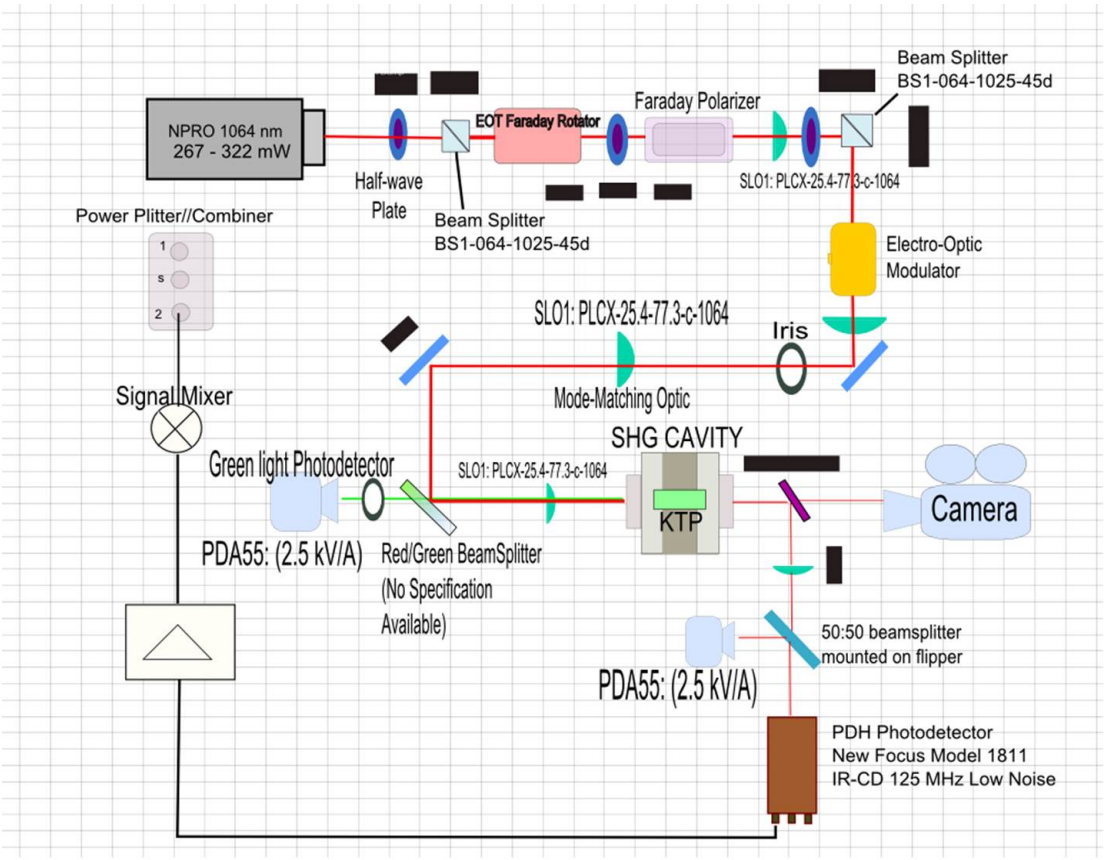

Figure 2: Optics Set-Up

,

The optics set-up contains four essential components. The first is the Faraday isolation and attenuation stage. A Faraday isolater prevents back reflected beam from interfering with the laser and half-wave plates modulate the beam intensity going out into the rest of the optics set-up. The second stage is the PDH servo (see section 2.3), which consists of an electro-optic modulator, the New Focus Model 1811 photodetector, the piezo actuator in the SHG, and a number of electronics that do not interact with the beam. The servo, as will be explained in section 2.3, locks the cavity in a resonator mode. The third stage is the cavity itself and a set of mode-matching optics which shape the beam to optimize the coupling of the beam mode with the cavity mode. Finally, the fourth stage consists of photodetectors, camera,

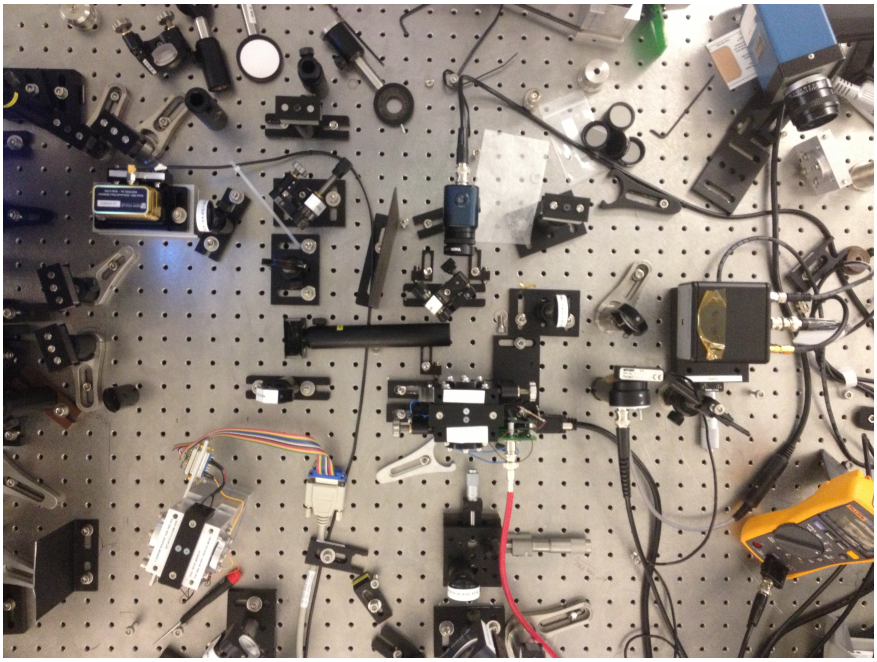

Figure 3: Bird's Eye View of Optics Table

and electronics to monitor and analyze beam energy and shape at various locations in the setup. A detailed list of the resources employed in the experiment can be found in appendix 1.

2.3 Alignment Improvements

The first step to achieving resonance is establishing the physical orientation of the beam and SHG cavity so that the waist size of the beam is optimized. A more detailed analysis of this can be found in Medina; *Characterization of SHG for Advanced LIGO*. The second aspect is to ensure the beam shoots through the central square aperture of the copper blocks in as parallel path as possible. This has been facilitated with a custom made set of aluminum beam-alignment markers:

,

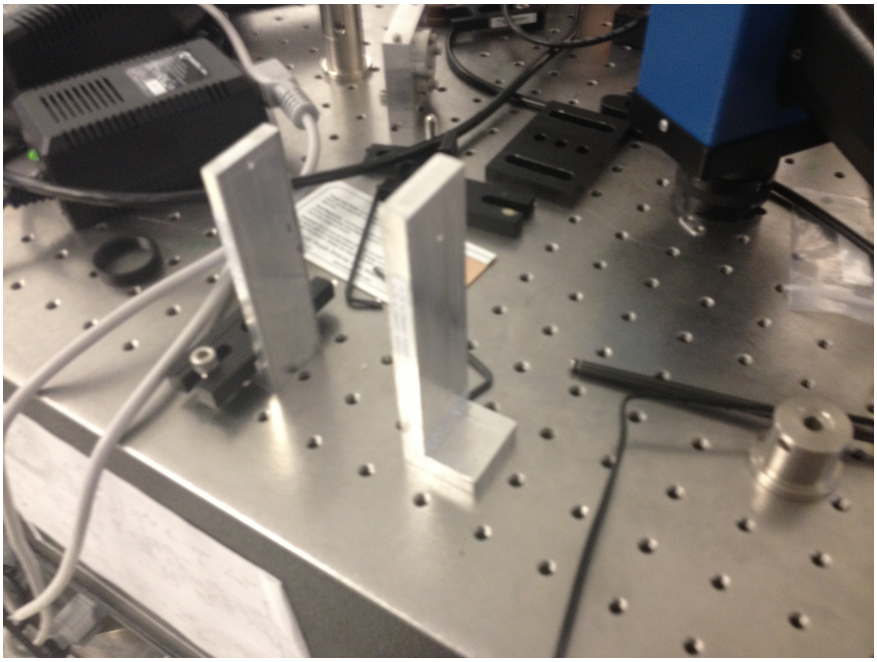

Figure 4: Beam Alignment Markers for SHG Cavity

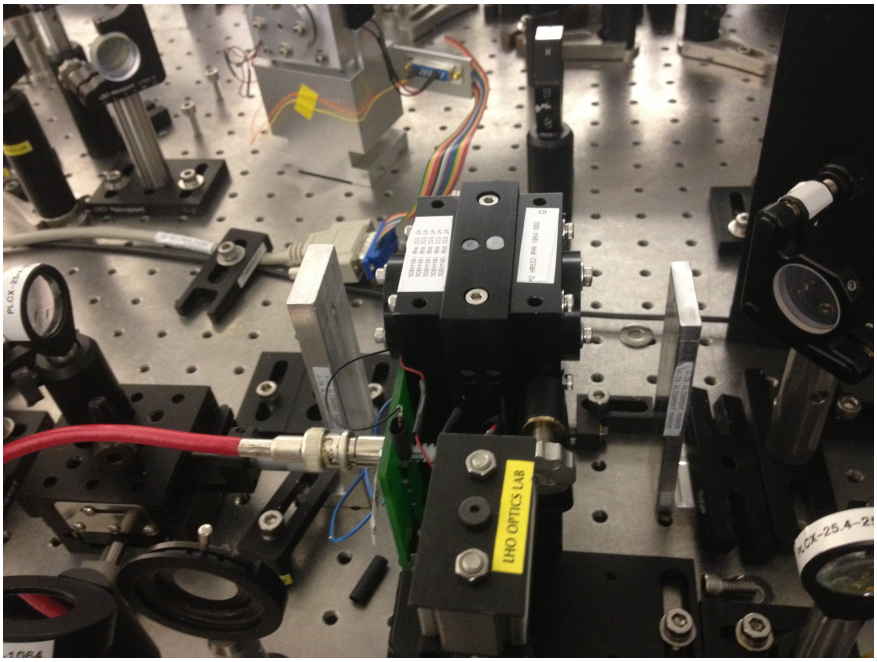

Figure 5: Beam markers with SHG

,

These markers have 2-mm holes drilled at the precise height to align with the input and output apertures of the cavity. They can be spaced arbitrarily far from the cavity, which forces the beam alignment to be very precise in terms of position and angle with respect to the cavity.

2.3.1 New SHG Design

The old SHG, (SHG 1.0) was difficult to align and assemble. A redesign of the old SHG model was drawn up (in SolidWorks 2013) and implemented to decrease the alignment time. The old SHG is shown below:

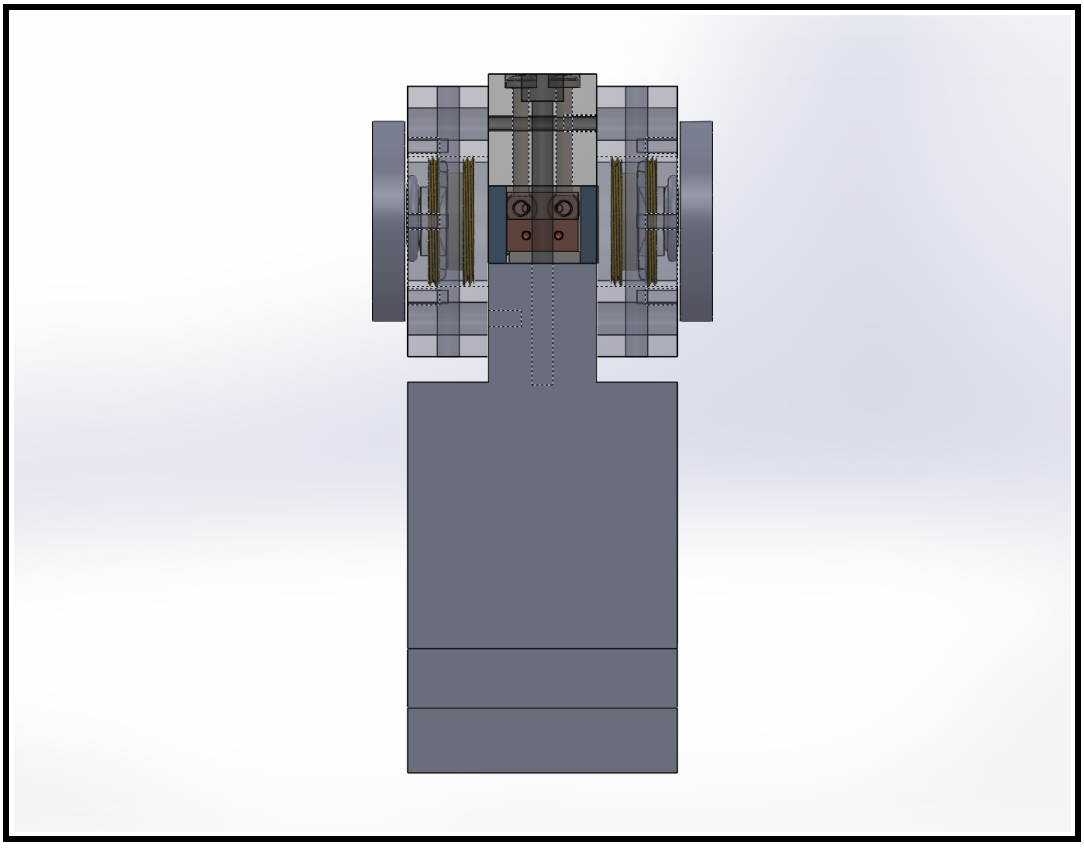

Figure 6: SolidWorks 2013 View of the Old SHG (v. 1.0)

,

The new SHG's main feature is a set of precision horizontal translation

stages for the forward and rear mirrors. These stages are adapted from lens-holders found in the optics set-up. To allow for bidirectional adjustment, a metal sheet spring is placed on the opposite end of each adjustment piece. Components of the horizontal translation stage are attached with screws and are entirely removable once the alignment is complete. The benefit of the stage, however, is not just limited to adjustment. The stage will 'preserve' the location of the mirror holders. If the mirror holders are removed and put back, they will fit effectively where they were last left. Thus, once the cavity is resonated once, adjustments can easily be made to the mirror mounts without realigning the cavity (apart from simple adjustments to the beam).

,

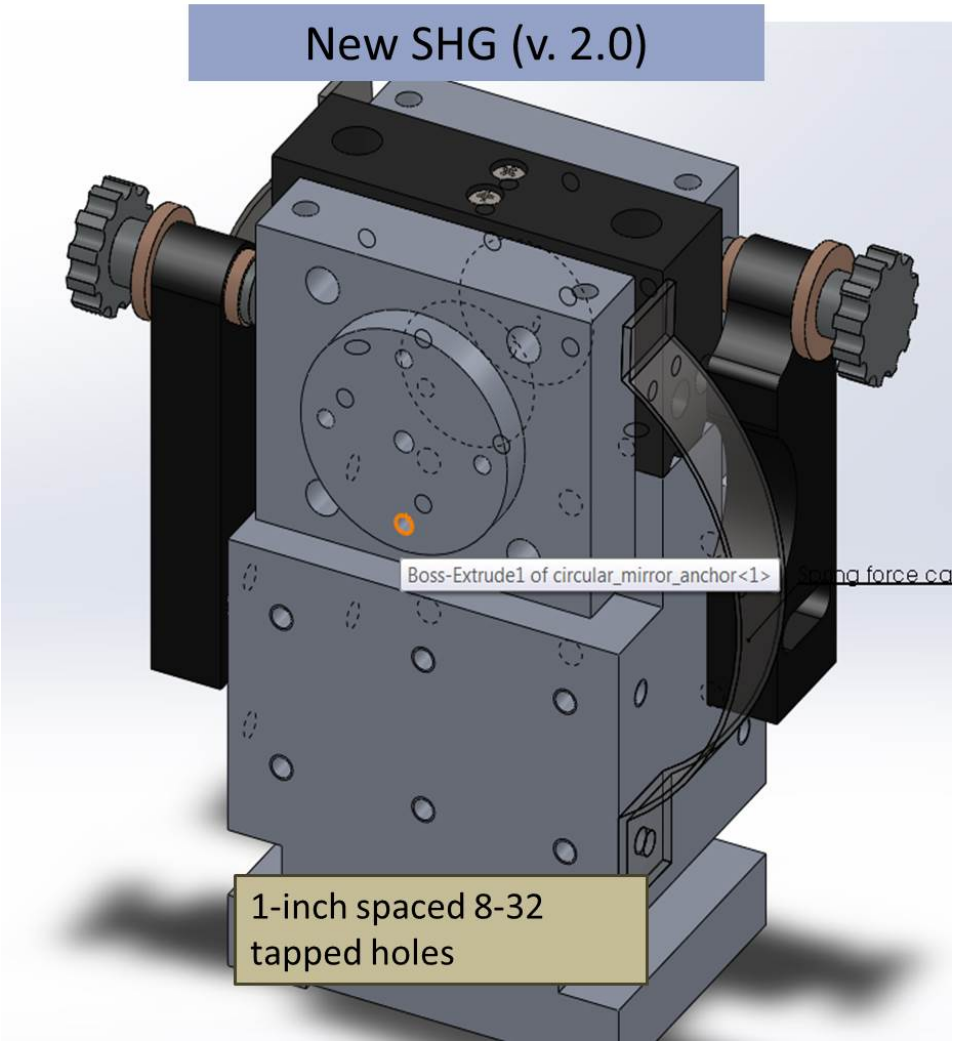

Figure 7: Isometric View of SHG Cavity with Horizontal Stages

,

Secondary features include detachable connections for the piezo-wiring and temperature control wiring so that the input mirror can be removed without having to unsolder any wire connections. In addition, a set of 8-

32 tapped holes have been incorporated into the front and back end at one inch vertical and horizontal spacings to anticipate future improvements to the SHG. And to improve pre-alignment installation, the thermistor ports on the copper blocks were enlarged an grooves were put in the delrin bridge and the brass mirror holder rings to allow the wires to be conveniently fed through and out. All design changes have been documented in SolidWorks 2013 for future reference and production.

The design changes have significantly decreased the alignment time for a given SHG cavity. The first cavity took a month to fully resonate. The new cavity took just three days (with appreciable improvements in successive alignment). Furthermore, characterizing the cavity with and without the crystal is now highly convenient because the horizontal adjustment stages preserve the resonant position. The alignment procedure accompanying the mechanical design changes can be found in appendix B.

For future SHGs, the design changes can be implemented manually on site or sent out to a machinist. Manually, all the parts for the horizontal stages are available at LIGO and are enumerated below:

1. two lensholders
2. two strips of stainless steel

Modifying and building the stages is not troublesome and does not require significant machining experience. If these parts are to be manufactured externally, then a new set of design drawings should be drawn-up to optimize the configuration.

2.4 Cavity Resonance

The SHG cavity can be modeled as a simple passive optical cavity. The resonator modes of the cavity occur when a beam bouncing inside the cavity reproduces its spatial electric field distribution after each round trip (with a loss of power with each round trip). If a sinusoidal EM signal is incident on the input/entry mirror, the field being bounced around inside the cavity consists of the transmitted incident signal and a contribution from the past circulating signal that has already traversed the cavity once and is coming back towards the entry mirror. This net field has the form:

$$\tilde{E_{circ}} = jt_1\tilde{E_{inc}} + \tilde{g_{rt}}(\omega)\tilde{E_{circ}} \tag{15}$$

$\tilde{g_{rt}}$ is the net round-trip gain for one transit cycle and t is the transmission coefficient of the mirror (j is $\sqrt{-1}$).

$$\frac{\tilde{E_{circ}}}{\tilde{E_{inc}}} = \frac{jt_1}{(1 - \tilde{g_{rt}})} \tag{16}$$

In a passive optical cavity,the axial (longitudinal) modes occur whenever the round-trip phase condition is satisfied:

$$\phi(\omega) = \omega p/c = 2\pi q \tag{17}$$

where q is an integer and $p = 2L$ with L being the cavity length. And of course, the amplitude distribution must also retain the same shape after each round trip transit. The longitudinal modes define the cavity's standing wave condition, restricting what frequencies can be resonated along the optical axis of the cavity. The frequency spacing of the axial modes is defined by the free spectral range ($\Delta\nu_{fsr} = \frac{c}{2nL}$; since the cavity has air as its medium, n = 1). For the SHG cavity, this value is roughly given by:

$$\frac{c}{2L} = \frac{3 \times 10^8}{2 \times 0.050} = 3\,GHz \tag{18}$$

In addition to the longitudinal spacing, there are modes that define the transverse distribution of the beam, the TEM_{mn} modes. The indices m and n describe the number of spots of zero illumination in the x and y directions respectively. In the SHG cavity, the design is such so that the cavity modes are Hermite-Gaussian modes (spatial field distributions specified by Gaussian).[3] With the transverse mode terminology, axial modes can be defined as TEM modes with n = m = 0 ([12]). As one further level of complexity, the free spectral range defined previously actually depends on the additional detail of the Guoy phase shift, which any Gaussian beam acquires as it travels in space. Thus:

$$\Delta\nu_{real_spacing} = \Delta\nu_{fsr}(\frac{\phi_G}{2\pi}) \tag{19}$$

where ϕ_G is the Guoy phase acquired per round trip.

[3]Gaussian beams retain their distribution as they propagate in space, have maximum spatial coherence, and smallest achievable spot size

,

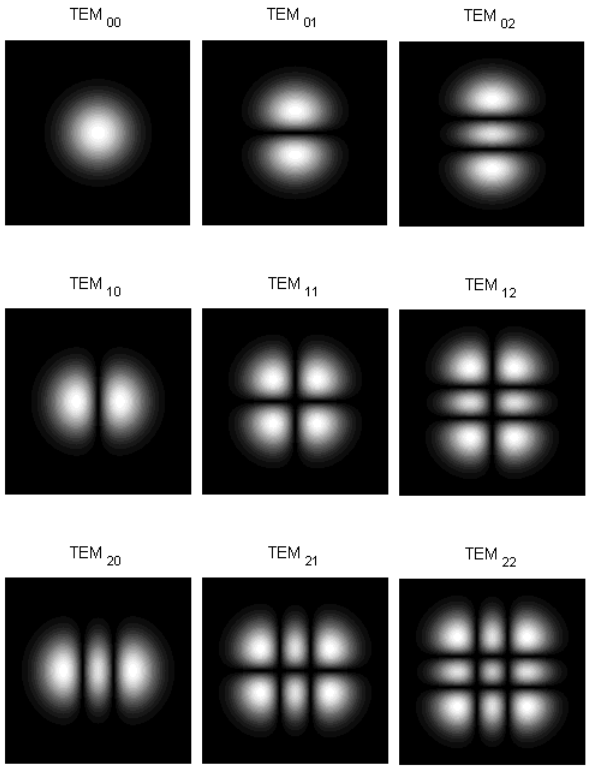

Figure 8: Hermite Gaussian TEM_{mn} modes

,

To resonate the cavity, the SHG's PI piezo-actuator was driven by a periodic triangle wave delivered by a function generator and amplified by a TREK piezo driver. The piezo-actuator effectively 'scans' the cavity for the resonant modes, generating a holistic survey of the behavior of all the excited modes of the cavity in real time. Any alignment changes in the optics set-up or the SHG is almost immediately apparent. For this experiment, a wave frequency from the function generator of 0.5 Hz is good for scanning.

The 'scan' also facilitates mode matching. Three plano-convex lenses in the SHG set-up focus the beam so that it can couple into the lowest transverse mode of the cavity (TEM_{00}). The last of which is placed on two translation stages for z and y tuning (z is along the beam direction). Without this, higher transverse modes can be excited and reduce the conversion efficiency from IR to green (with the crystal in the cavity). To get a statistical sense of the mode mismatch, take the ratio of the higher order mode signal amplitude over the maximum transmission peak (00 mode). For this experiment, the mode mismatch was reduced as far as 5

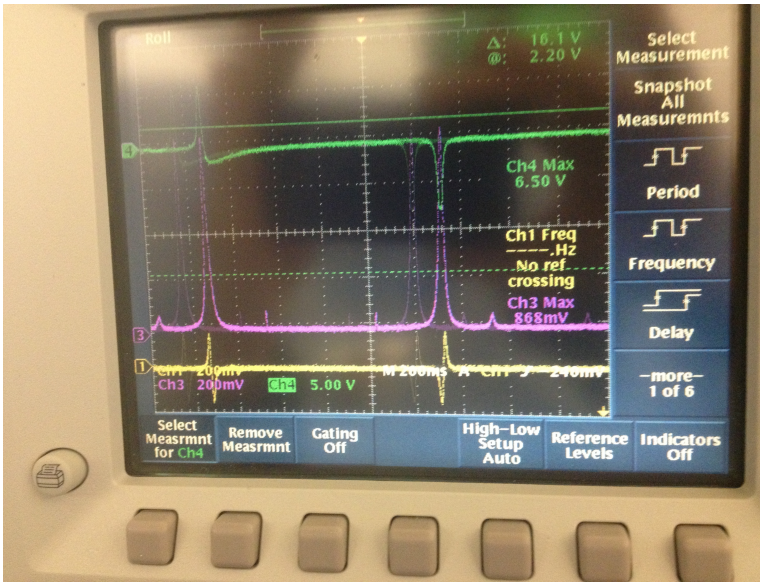

Figure 9: oscilloscope trace showing scan with piezo: purple = transmission of infrared, yellow = PDH signal, green = control signal

Figure 9 shows an oscilloscope trace of the cavity being scanned. the IR transmission in purple with the peaks being the TEM00 modes as they are scanned by the piezo. The error signal is in yellow right below, characterized by its clear anti-symmetric pattern about the resonance peak. The control signal is measured in green, but has little physical significance since the cavity is not being locked on resonance. Optimal alignment is achieved when the transmission peaks of the 00-mode are optimized and the transmission of the smaller higher mode peaks are minimized.

2.5 Cavity Stabilization: Introduction to Pound-Drever-Hall

The SHG requires stability in the input beam frequency in order to maintain a constant green beam output. However, random fluctuations in the laser's frequency means a fixed-length cavity will fall in and out of resonance, which is undesirable. A servo 'measures' or senses the difference between the resonant frequency and the actual laser frequency (the difference will be denoted δf) and adjusts the the length of the cavity to maintain resonance (PDH

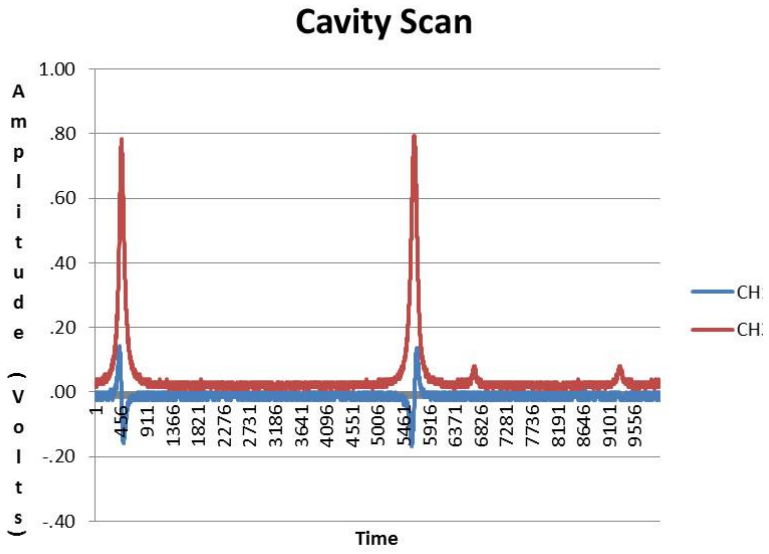

Figure 10: Computerized waveform capture of oscilloscope trace; time scale is roughly 1 second (period of the signal = 0.5 Hz)

is normally used to directly stabilize laser frequency, but is used here to stabilize the resonance of the SHG cavity).

The main problem of the servo is identifying which side of the resonance peak the cavity (length) is on (i.e. whether the cavity should be shortened or elongated). Naively, if an error signal was derived by the difference of the peak resonance transmission and the actual transmission, the signal is always greater than or equal to zero. To measure δf, pre-PDH servos using the reflection properties of the cavity (which depends on the frequency of the incoming light), but since the reflection coefficient is symmetric about resonance, there was no way to tell which side of the resonance the cavity was at. This problem was originally resolved by adding an offset to the reflection signal, but made the system sensitive to intensity noise.

The clever solution of PDH is to make an indirect measurement of the derivative of δf using the reflected beam at the input mirror of the cavity [9]. The reflection coefficient is sensitive to δf, and is given by:

$$F(\omega) = \frac{r(e^{\frac{i\omega}{\Delta\nu_{fsr}}} - 1)}{1 - r^2 e^{\frac{i\omega}{\Delta\nu_{fsr}}}} \tag{20}$$

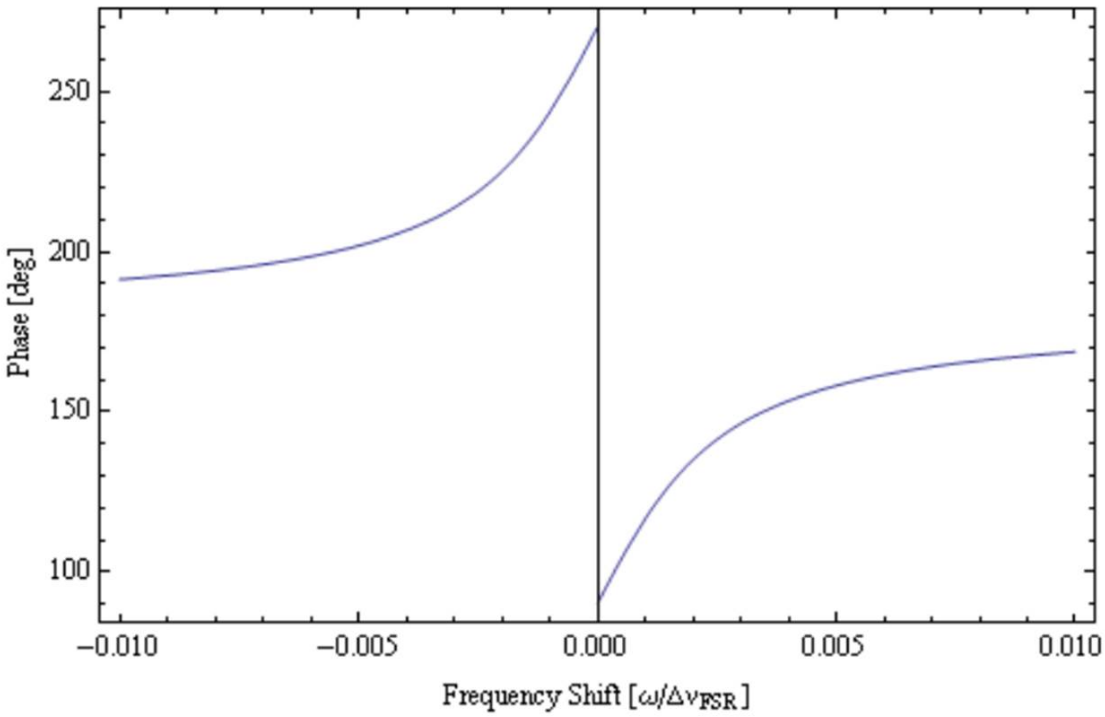

Figure 11: Plot of Reflected Beam Phase versus Frequency

[1]

where r is the reflectivity of the mirror and $\Delta\nu_{fsr}$ is the free spectral range, or the frequency spacing of the resonant modes. [5]. At resonance, the term $\frac{\omega}{\Delta\nu_{fsr}}$ is an integer multiple of 2π and the reflection coefficient becomes 0. Off resonance, the numerator is nonzero and the reflection coefficient increases, getting larger the farther away from resonance the cavity gets. Take the derivative of this function with respect to ω and one can note that it is antisymmetric about resonance.

The PDH servo actually looks at the phase of the reflected beam, which has a function that looks similar to the derivative of $F(\omega)$ as shown in figure 11:

In either case, the anti-symmetry about the resonance holds the information as to shorten or lengthen the cavity. What the PDH servo does is introduce frequency sidebands to the laser-light via an electro-optic mod-

ulator. In principle, these sidebands are reflected off the cavity while the carrier enters the cavity. Some of this carrier beam will eventually leak back out with a phase shift relative to the sidebands. [9]. This signal is sent to a photodiode which converts it into an electrical signal mixed with a local oscillator (LO) in phase with the EOM modulation signal. The crucial point is that the output of the mixer has different signs on either side of the resonance, and this is what constitutes the PDH control signal. In practice, the signal is passed through a pre-amplifier (SR560) so high frequency jitters in the signal can be filtered out and the remaining signal is amplified by a factor of 10-100 (or more). In effect, the servo is a PI control. The gain in the signal functions as the proportional control; the low pass filter integrates the signal for pseudo-integral control. [4]

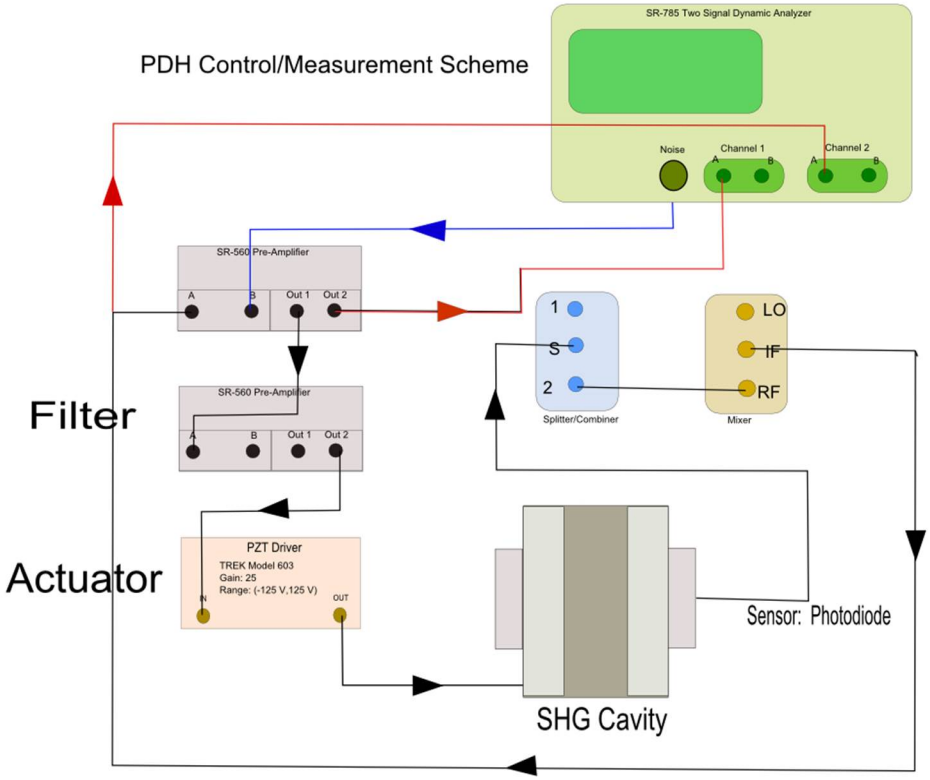

Figure 12: PDH Servo Set-Up including connections to Measure the Frequency Response on a SR-785 Signal Analyzer

[4] real integral controllers guarantee a pole at zero, but the pre-amp does not

,

3 Results

3.1 Resonance Locking and Stability

The settings on the pre-amplifier are important to maximize performance:

- High Dynamic Reserve
- Low Pass filter at 1 hertz (or lower)
- DC coupling
- Invert off (invert will change sign of control signal

3.1.1 Beam Stability

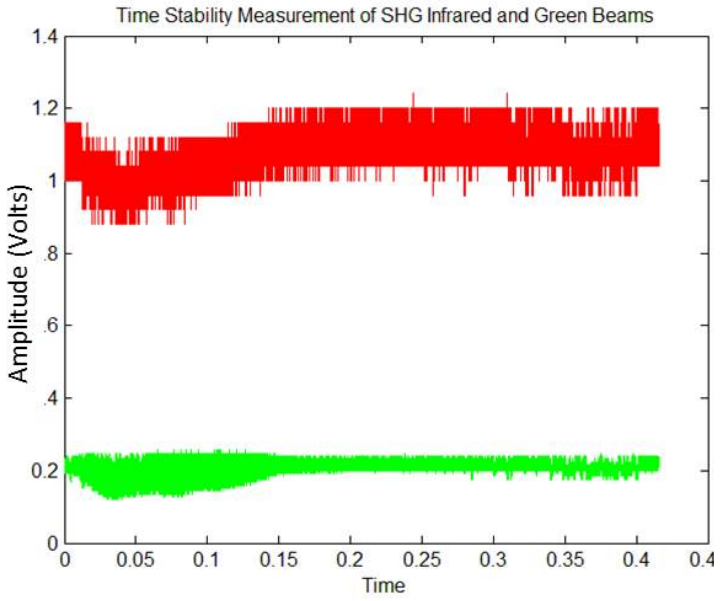

Figure 13: Oscilloscope Trace of Voltage Beam Intensity vs. Time. Note that the gains on the photo detectors are different so a conversion efficiency measurement cannot be extracted from this diagram

The graph shown in figure 4 is an oscilloscope trace over one and a half hours with each 0.005 unit of time equivalent to about 10 seconds. The

extended time trace was produced by a MatLab (Instrument Control) program and a RS-232 connection to a Tektronix TDS 210. This measurement was taken in the early alignment stages of the cavity, where resonance was achieved, but the cavity was not securely locked down. The hour-long trace shows high noise for the infrared beam and a possible increase in amplitude noise for green light whenever the strength of the infrared beam dips below a certain point. Considering the noise levels, a second graph measuring the averages of the power was plotted over time:

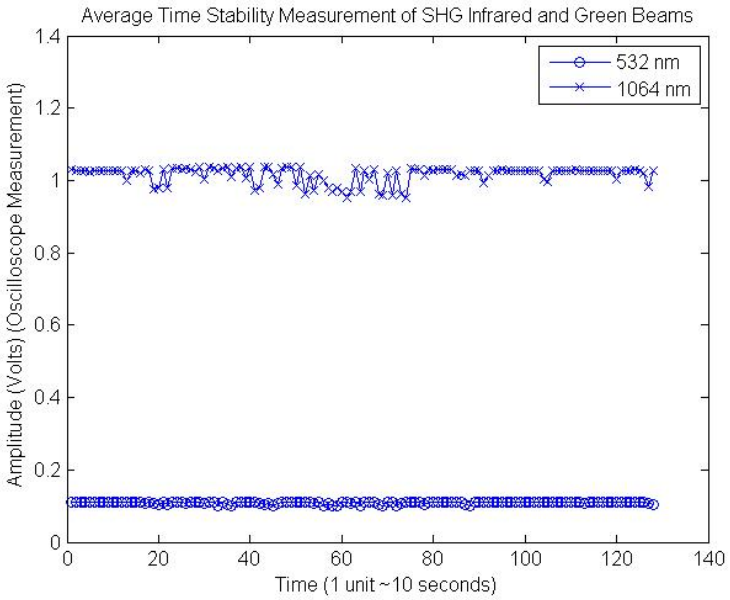

Figure 14: Average Green and Red Power

,

,

This shows that on average, the power of the beam is fairly stable even with the mechanical instability of the SHG. In fact, it even seems that the green light is, on average, more stable than the red beam. In any case, the amplitude "noisiness" of the beam can be reduced by tightening the screws connecting the mirror holders to the delrin bridge and SHG base. The noisiness can be attributed to thermal effects, circulating air, and vibrations on the table. A second set of measurements with the cavity structurally secured suggests that the cavity does become more impervious to environmental fluctuations.

,

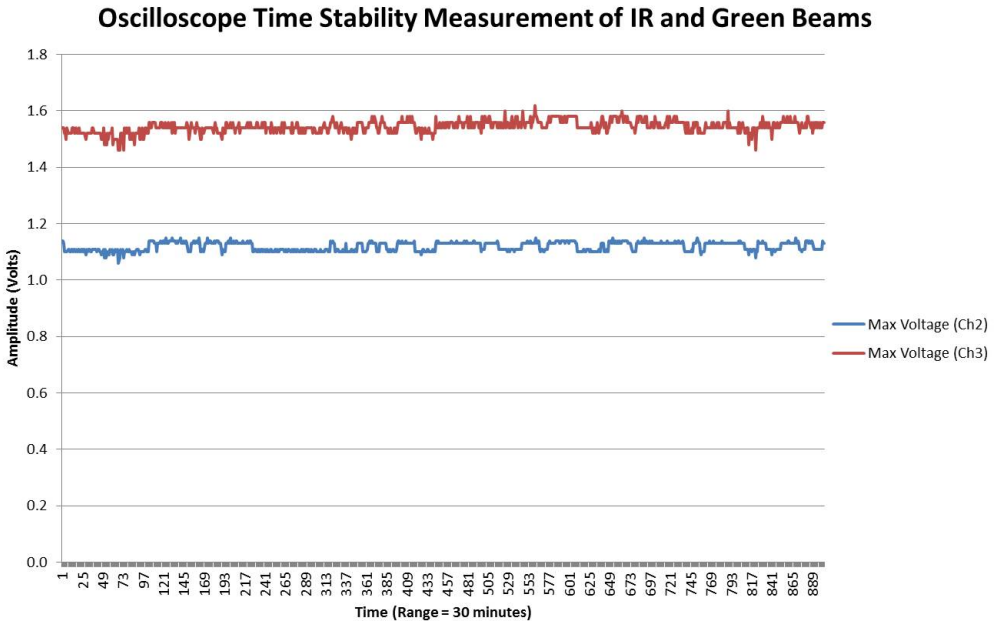

Figure 15: Oscilloscope Trace of IR and Green beams in SHG with cavity structurally secured (screws tightened) AND Temperature Control On; Max Voltages Plotted

,

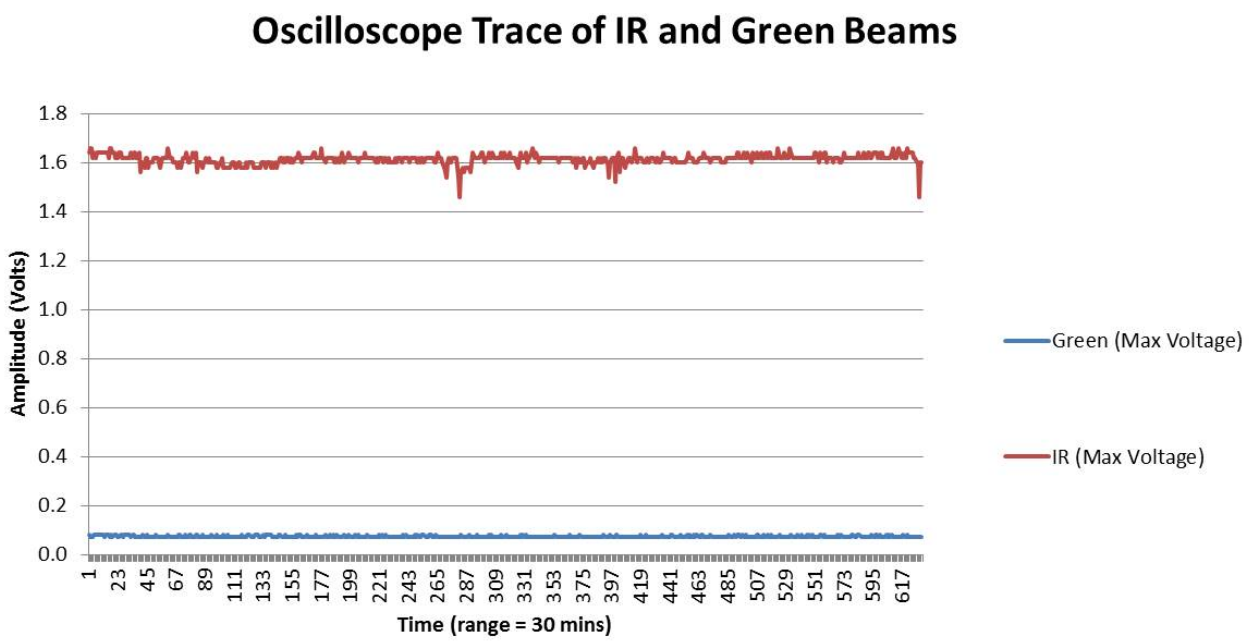

Figure 16: Time Series of IR (red) and Green(blue) Without Temperature Servo

,

Here, the standard deviation of the IR beam is 0.0204 volts, but for the green beam, it is 0.0042 volts. This difference between the standard deviations is significant, but further tests should be done to verify that the servo is really not introducing the extra 'noise' at higher green output powers [5]. The next step is to replicate this result with a direct measurement of the power. [6]

A second visualization of the beam stability is a histogram of the beam's power in the time measurements. Several of these measurements reveal that with a good lock, the beam's power does not fluctuate significantly.

[5] As in section 3.2, the fluctuations in the temperature servo once it reaches its set temperature is on the order of 1/1000 of a degree Celsius, which is pretty small

[6] Using Ophir Vega, refer to appendix for data

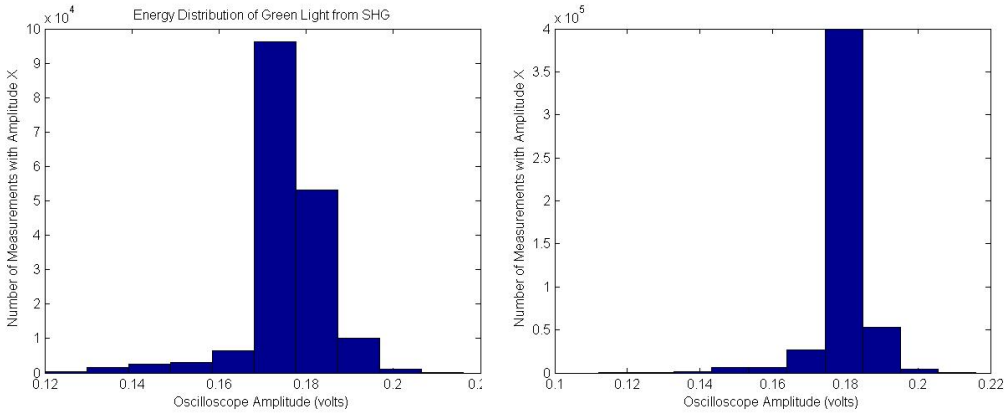

(a) Short Sample: 1 minute (b) Long Sample 30 minutes

Figure 17: Green Beam Power Distribution as Measured on Oscilloscope

,

However, if the lock drifts (i.e., the beam power spends an appreciable amount of time off the peak transmission), the histogram distribution becomes discontinuous (some of the bins show no measurements) as shown in figure 18:

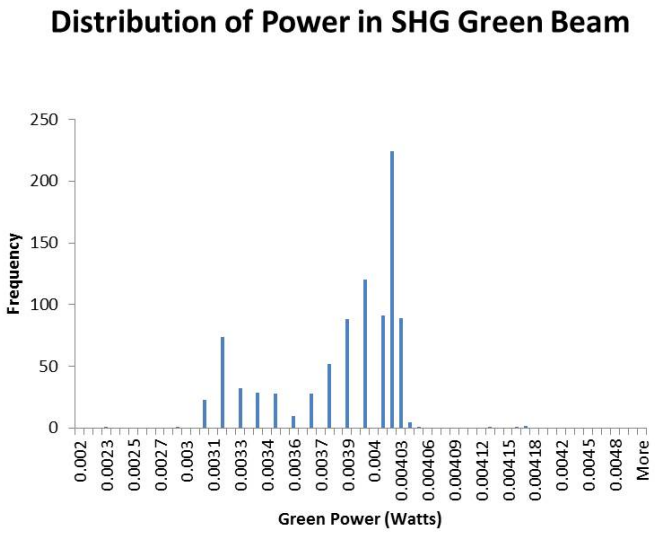

Figure 18: Green Power Sampling Distribution with Discontinuities

,

The discontinuous distribution measured above could be a result of a slow sampling time (this was via a power meter taking samples every second). An alternative explanation is that the beam power is actually jumping as the lock drifts between different. Two things must be done to confirm this. One is to increase the samples per unit time. The second is to characterize how laser beam intensity itself fluctuates.

,

3.1.2 Behavior of Control and Error Signal

Another stability problem is the behavior of the control signal, especially when the servo loses lock. As shown in figure 19, the lock of the servo is broken as the control signal grows continuously larger in peak amplitude. At a first glance, this could be an issue with the integral control signal.

$$C_{integral} = \int_a^b \epsilon(G_{int})\,\mathrm{d}t \tag{21}$$

Because of the time integration, the integral control signal will grow over time if the error signal does not zero out. However, the oscilloscope trace in figure 20 shows that the error signal is effectively 0 (albeit with a slight offset). The only other major explanation is the limited range of the PZT. If the PZT cannot produce enough control signal for an error signal, then the control signal will get bigger and bigger to compensate while the PZT responds less and less until the lock is broken.

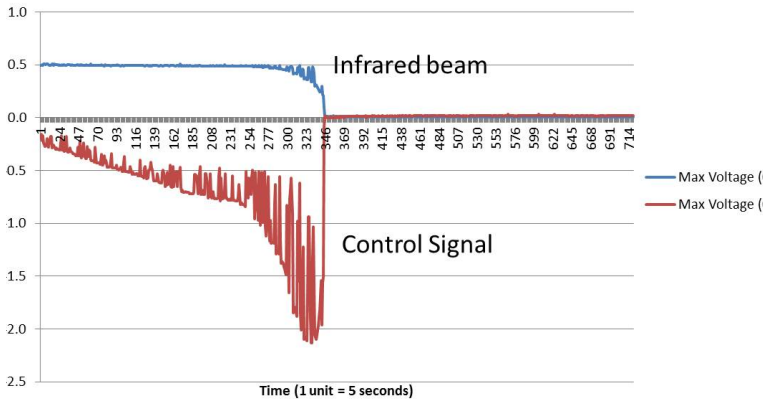

Figure 19: Graph of beam amplitude versus control signal amplitude on TDS 3034B over time.

One way to avoid this is to tune the resonance to the center of the piezo's range. That way, it maximizes the distance the cavity resonance has to drift before the servo loses lock, which is demonstrated in 20.The best way,

however, would be to get a high voltage amplifier (or piezo actuator) which can push the piezo through several free spectral ranges. The current options have ranges of 150 volts (0-150 DC) and 250 (-125 to 125 DC). However, the PZT in the cavity can take up to +700 volts.

,

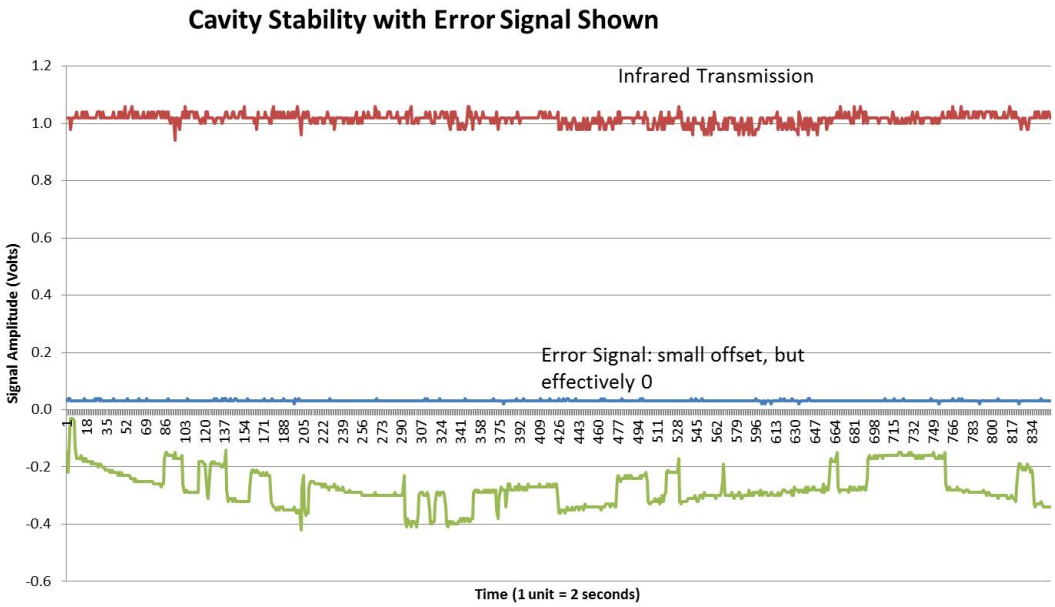

Figure 20: Time Series of PDH Servo with Error Signal

,

Though the IR transmission is stable in 20, there is still amplitude noise. Characterizing this noise to see if it can be further reduced is of interest. One contributing factor could be in the control signal. In figure 20, the control signal shows square shaped bumps, which might likely be the servo correcting for actual jumps in the laser frequency. To further correct for this, the laser frequency itself can be stabilized via a reference cavity (or technically another PDH servo).

3.2 Beckhoff Temperature Servo

A digital temperature prototype was installed and programmed on SHG 2.0 to enhance control monitoring of the KTP crystal temperature. The new temperature controller consists of four Ethercat terminals (which translates inputs from the TEC and thermistor to the computer and vice versa) and a current driver. Twincat software sets up a programmable logic controller in the IEC-1131 language standard and receives input and sends commands to the Ethercat bus terminals, which in turn takes input and feeds output to a thermistor and a thermoelectric cooler (TEC).

The new servo needs to be analyzed for response characteristics, which is greatly facilitated by the programming flexibility of the TwinCat software. A unit step response and a set-temperature response were measured in the time domain. The unit step was measured by sending a 1 volt step (Heaviside function in time) to the TEC and measuring the temperature change as a result. response is shown in the top figure below.

,

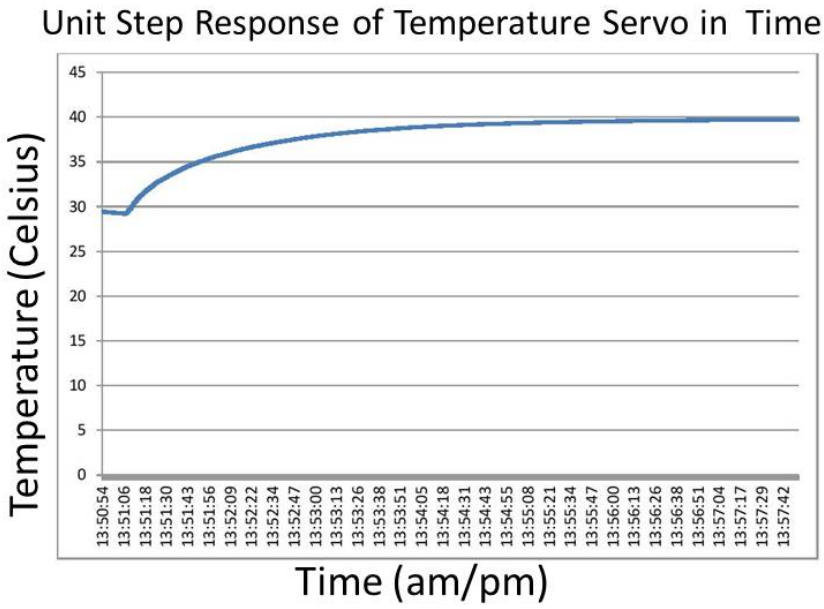

Figure 21: unit response of Beckhoff Temperature Servo

,

This unit response looks like a decaying exponential. If we consider the time response of a first order system with transfer function H(s), its time response looks like:

$$H(0) + (H(\infty) - H(0))e^{\frac{-t}{\tau_0}} \tag{22}$$

[3] which is effectively the time response measured for the Beckhoff temperature servo. The time response is basically derived by taking the inverse Laplace transform of the convolution of the unit step function (in frequency space) and a transfer function approximated as:

$$H(s) = \frac{bs + c}{s + a} \tag{23}$$

and the Laplace transform of the unit step function is:

$$\Gamma(s) = \int_0^\infty \gamma(t)e^{-st}dt = \int_0^\infty e^{-st}dt = \frac{1}{s} \tag{24}$$

[3]

$$Y_{conv} = \frac{1}{s}H(s) = (\frac{1}{s})\frac{bs + c}{s + a} \tag{25}$$

,

A more practical measure of the servo's response is to simply see how it reaches a given set-temperature (shown below in figure 22). The first graph shows that the servo overshoots the set temperature once and stabilizes. Compared to a response where it smoothly reaches the set temperature like the unit step response, this overshoot actually shows a faster settling time. Modulating the UGF roughly shows that higher UGF correlates with a faster rise time, but a more thorough investigation should be completed to confirm and verify the settling time, peak time, and overshoot for different UGFs as well as other parameters in the servo, such as the gain.

,

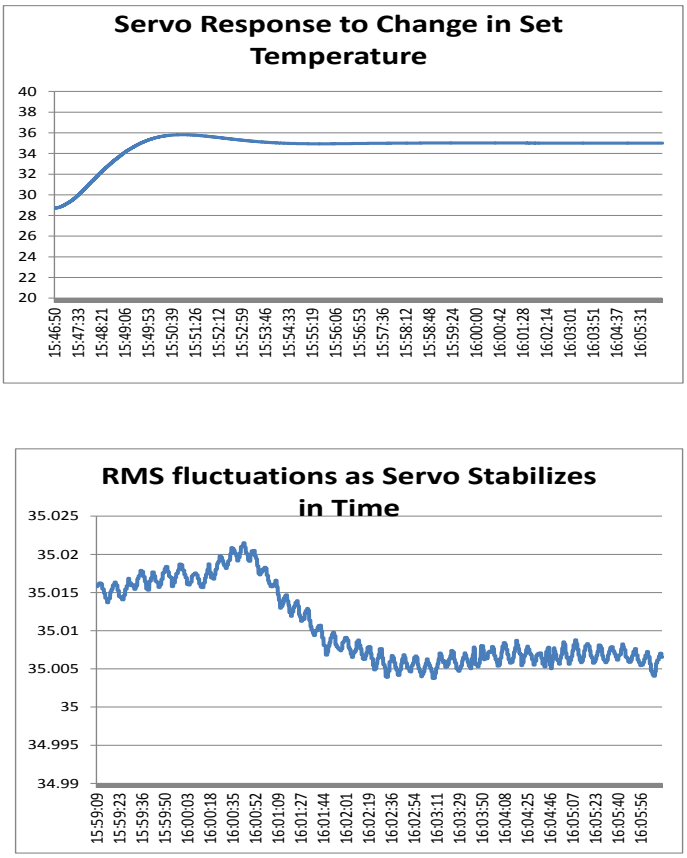

Figure 22: Set Temperature Response of Beckhoff Servo

,

The bottom graph of figure 22 shows the RMS fluctuations of the temperature as the servo approaches the set temperature. Nothing anomalous appears and confirms that the servo remains fairly stable in time. In addition, the overshoot for this response is only about 3.3%, which is much less than the upper limit of 10%. Finally, the second graph of figure 16 shows the minute fluctuations in the servo as it settles down on its set temperature. This graph looks reasonable and does not show any major anomalies.

Table 1: Time Characterization of Temperature Servo (with Single Overshoot

Rise Time	3 mins.
Settling Time	6 mins.
Overshoot	1 degree Celsius or 3.3% of set temperature
Peak Time	4.5 mins.

,

3.3 Temperature Tuned Phase Matching

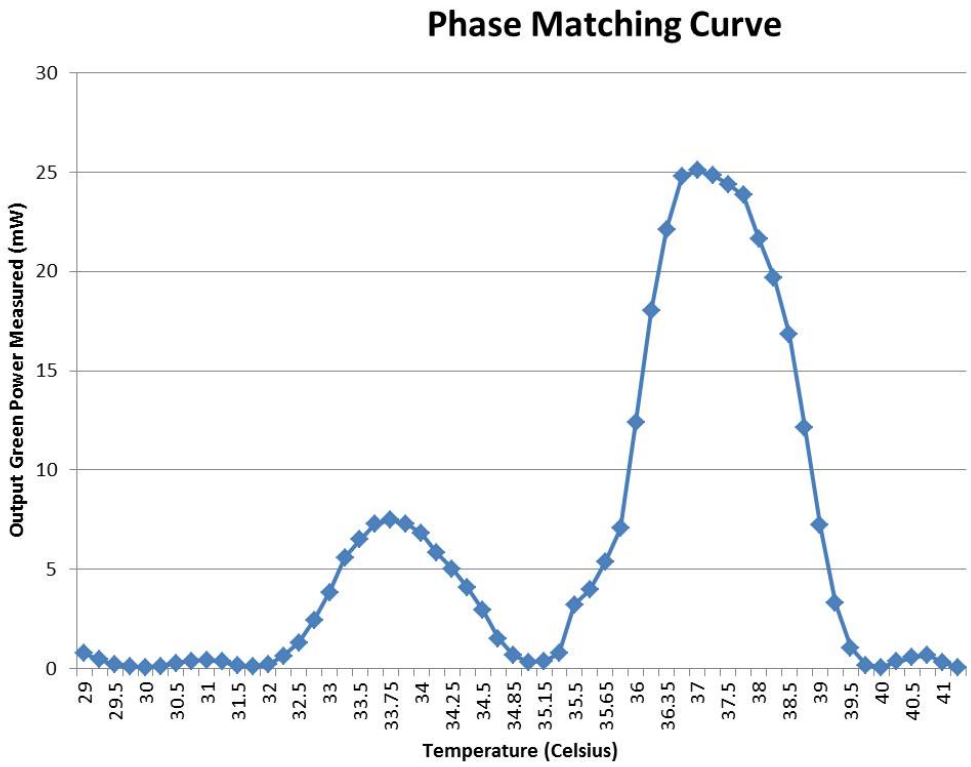

Figure 23: Green Power of SHG as a Function of Temperature

,

The phase matching curve shown in figure 23 was acquired with the crystal in the resonant cavity. Each measurement involved adjusting the temperature in fixed increments and tuning the piezo-actuator such that the cavity achieves resonance. The plot shows that the phase matching looks roughly like a sinc-squared function derived in the introduction and background, but has an anomalously large secondary peak at 33.75 degrees Celsius in addition to the primary one at 37.5 degrees. The effect is likely due to pump depletion, considering that crystal is in the resonant cavity. To get a more accurate phase matching curve, the experiment needs to be done without the cavity (single pass) [7]. But for all practical purposes in aLIGO, the crystal needs to be held at its optimal temperature, which can be scanned for via the temperature controller.

3.4 Conversion Efficiency by Increasing Input Infrared Power

Besides phase matching, which was achieved by temperature tuning, increasing the input power also increases the conversion efficiency. Theoretical predictions show approximately that at low powers, the output green power scales quadratically with input red [10].

$$P_{red} = \eta P_{green}^2 \tag{26}$$

where η is the ratio of $\frac{P_{green}}{P_{red}}$. One measurement on SHG 1.0 was done with two separate power meters to measure green and red power separately. But because two different power meters were used, the two were checked against each other to see how much the measurements are off relative to each other. Three measurements were done with both meters at low (20 mW), medium (100 mW), and high (150 mW) infrared power. The mismatch in the infrared readings were roughly between two and ten percent, which was deemed okay to proceed. The first result is plotted below.

,

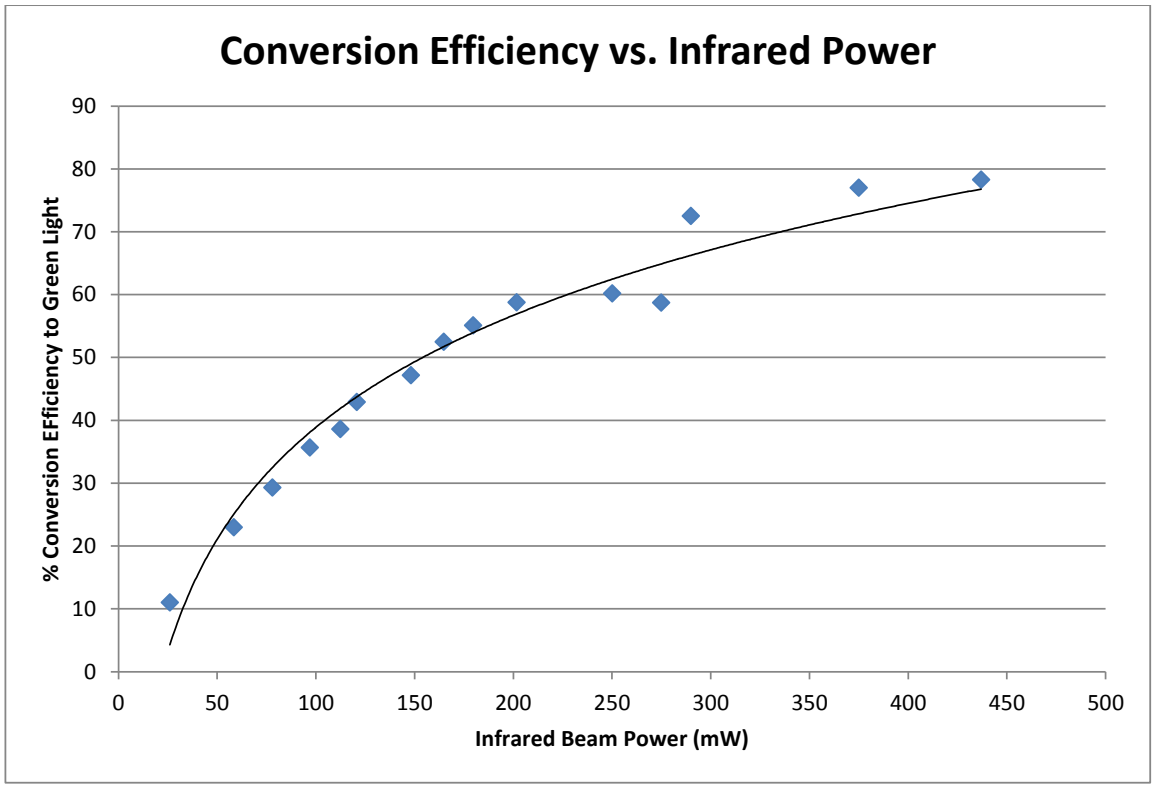

,

the plot shows conversion efficiency as a function of input infrared. The plot appears to be approximately logarithmic or a function of the form: $k - \alpha e^{-\beta P}$), which is consistent (at least visually) with findings from Medina's findings [8]. The maximimum observed conversion efficiency on SHG 1.0 was 79% at 475 mW of IR, which is much higher than the prediction from Medina. A similar conversion maximum conversion efficiency was similarly measured on SHG 2.0.

A second plot with green power as a function of infrared power shows that the second harmonic power scales quadratically with input power, which follows theoretical predictions in the equations shown below. In reality, pump

depletion must be accounted for which modifies the equation slightly to:

$$P_{2\omega} = P_{\omega} tanh^2(\sqrt{\alpha_{SHG} P_{\omega}^2}) \tag{27}$$

Much more experimental modeling can be used to verify the accuracy of the experimental measurements, but will require more measurements with the crystal outside the cavity. Additionally, one potential problem with this measurement is that for each data point, the crystal temperature was not tuned to maximize the green efficiency. Especially at higher beam powers, there is likely additional heating from the laser beam hitting the crystal. Ideally, the thermistors should register this heat and adjust appropriately, but since the thermistors are not in direct contact with the crystal, thermal effects from the laser could be nontrivial (even if small).

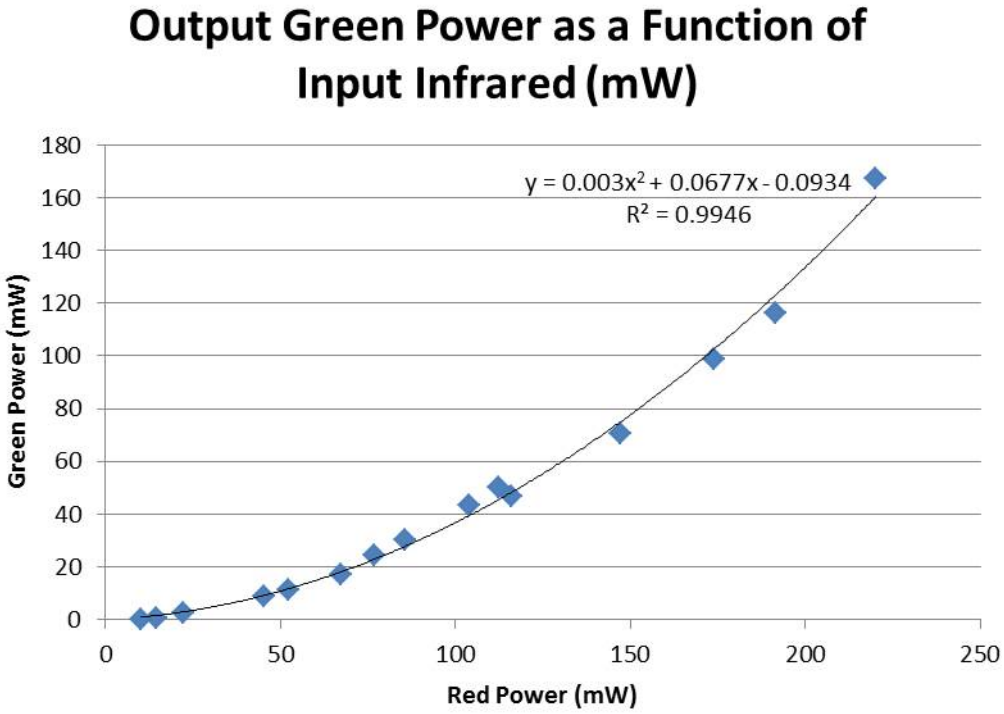

Figure 25: Output Green Power as a Function of Input IR Beam Power

4 Conclusions

A set of mechanical design improvements have vastly decreased the work and time needed to align the SHG cavity as well as introducing the freedom to adjust the cavity once resonance is found without requiring full re-alignment. Instead of a month-long endeavor to produce a stable alignment, the process can now be completed in under a day or several hours (with practice or skill). The design changes are implementable with materials already available at LIGO and simplistic enough for anyone with basic machining experience to reproduce.

Characterization of servo stability suggests that the locking is not as good as previously stated in Medina et. al. Though the servo locks, there is a problem posed by the piezo actuator running out of range in addition to other possible instabilities which have not yet been identified. The first problem can be mitigated with a piezodriver which can drive the piezo over multiple free spectral ranges, especially considering that the piezo actuator can receive up to 700 volts and is currently only getting 150 volts (for the ThorLabs driver; the TREK does 250, that only covers 1250 nm, which has one free spectral range). Apart from that, the servo has fairly good stability which can be improved by reducing frequency noise from the laser by locking it onto a reference cavity.

A Beckhoff temperature controller has also been fully installed and is functioning well, capable of holding a stable temperature almost indefinitely. The controller also has functionality to record voltage delivered to the thermoelectric cooler and the temperature measured by the thermistors, which can be converted to Excel format and plotted. It has been demonstrated to be a suitable replacement for the ThorLabs TED 200C. Further work on the temperature controller would be to incorporate integral and differential control in the TwinCat source code.

Conversion efficiency of the SHG has been measured up to 79% IR to green at 0.500 watts of IR input power. More measurements should be taken to confirm this statistic (such as measuring the extent of the pump depletion in the cavity at high power). In addition, a model should be computationally constructed from Z.Y. Ou's paper, which will confirm that the behavior of the input power and green power match the theoretical predictions. If the theoretical and experimental data do not match well, then a second measurement should be taken with temperature tuning at each measured point. The coupled achievements of high conversion efficiency and alignment improvement

and stability produce an effective SHG unit for use in aLIGO.

An important future characterization of the set-up is the noise in the green and IR beams. With a continuous wave, single frequency laser, frequency and phase noise must be considered in addition to technical sources of noise from vibrations on the table, noise from the pump, etc.

Appendices

A Resources in Experiment

1. piezo actuator
2. NPRO 1064 nm continuous wave laser from JDSU (part M126N-1064-700)
3. SHG CRYSTAL: Periodically poled KTP
4. TREC piezo-actuator/voltage amplifier Model 603
5. Tektronix Oscilloscope (TDS 3034B and TDS 220)
6. Stanford Systems; Function generator (Model DS340)
7. Stanford; Low Noise Pre-Amplifier (SR560);
8. 24480 kHz Electro-Optic Modulator Model 4003 New Focus
9. Half-wave plates
10. quarter wave plates
11. Stanford; Two signal dynamic analyzer (SR 785)
12. Hewlett-Packard (agilent) RF Spectrum analyzer (4395A)
13. Hewlett-Packard ESG-1000a signal generator
14. From Mini-Circuits Company:
    (a) Signal Mixer (ZAD 3H)
    (b) Power Splitter-Combiner (ZSC-1-2)
    (c) Directional Coupler (ZDC-20-3)
15. Model 1811 New Focus Low Noise Photodetector (50-125 MHz)
16. Connectors; BNC, SHV, SMB, SMA
17. ThorLabs Temperature Controller (TED 200C)
18. Beckhoff TEC Controller (pending)
    (a) TEC (Laird Technologies, Model Hot 20,65,F2A,1312)
    (b) EtherCat TEC Current Driver (D1201359-v1)

(c) Ethercat Terminals (EL3104 (EL3102 compatible),EL3692, EL4132)

(d) Ethercat Bus Terminal EK1101

(e) Thermistor (Mouser 71-4M3002-C330K thermistor, but the present thermistor is a 10k, recalibration is possible)

B Cavity Alignment Procedure

This procedure assumes that the optimal position of the cavity has already been determined based on desired waist size for the IR beam)

1. Place aluminum alignment markers on table and adjust position until IR beam passes through both.
2. Center Cavity on the beam and lock down
3. Fine adjustment of beam with the mirrors (input power on front side should be as close to exit power on other side)
4. Insert front mirror (M1)and insert screws & loosely tighten (do not have to install all screws, just enough for mechanical stability) and adjust position so that:
   (a) back-reflected beam follows same path as input beam (make sure there are not two spots on final mode-matching lens)
   (b) output power from the lens is roughly 10% of the input (M1 has reflectivity 90%)
   (c) a circular spot should be recorded by the output camera
5. Insert Rear mirror (M2) without screwing down. By hand, adjust position to see if the image on the TV flutters AND suddenly splits into a large number of lobes.
6. Regardless of if that happens or not, turn on PZT and have the actuator 'scan'
7. loosely tighten M2 and coarse adjust until flutter AND lobe splitting effect is seen. Now resonance is near (s
8. carefully adjust mirrors to see if fluttering can be increased and lobes better defined and decreased
9. alternate mirror and cavity adjustments until you find TEM 00 mode
10. note that transmission measured on New Focus 1811 photodiode should now peak at 00 or higher order modes.
11. adjust mirrors to achieve mode-matching

12. adjust the z and y position of last mode matching lens to achieve best mode-matching.

C Temperature Servo Script (IEC-1131)

```
0001 FUNCTION_BLOCK TECControllerFB
0002 VAR_INPUT
0003     Request:          SaveRestoreEnum;
0004     TECControllerIn:  TECControllerINStruct;
0005 END_VAR
0006 VAR_OUTPUT
0007     TECControllerOut: TECControllerOutStruct;
0008 END_VAR
0009 VAR_IN_OUT
0010     TECControllerInit:  TECControllerStruct;
0011     TECController:      TECControllerStruct;
0012 END_VAR
0013 VAR
0014     ErrorHandler:     ErrorHandlerFB;
0015     ConvertRtoT:      RtoTempFB;
0016     ErrorCheck:       ErrorCheckFB;
0017     PIServo:          PIServoFB;
0018 END_VAR
```

```
0001 CASE Request OF
0002     Restore:
0003         TECController:=TECControllerInit;
0004     Save:
0005         TECControllerInit:=TECController;
0006 END_CASE;
0007
0008 TECControllerOut.ThermControl.DisableAutoRange:=FALSE;
0009 TECControllerOut.ThermControl.Mode:=2;          (*2 wire measurement*)
0010 (*TECControllerOut.ThermControl.Range:=5;*)
0011
0012 (* convert counts to volts, amps, vice versa*)
0013 TECController.TECVoltageBack:=EL3104(TECControllerIn.TECVoltageReadback)/2; (*gain of 2 on voltage readback*)
0014 TECController.TECCurrentBack:=EL3104(TECControllerIn.TECVoltageReadback)/4;  (* 4 Ohms on current readback: I = V/R...where resistance =
0015 TECControllerOut.TECVoltageSet:=EL4132(TECController.TECVoltsOut*2); (* driver divides voltage by a factor of 2 before it is applied to TEC*)
0016
0017 IF TECControllerIN.ThermValue>1 THEN (* if statement is to avoid dividing by zero*)
0018     (* Convert from resistance to temperature, if thermistor data is invalid *)
0019     ConvertRtoT(Resistance:=TECControllerIn.ThermValue, Temperature=>TECController.ThermistorTemperature);
0020 END_IF;
0021
0022 ErrorCheck(TECController:=TECController, TECControllerIn:=TECControllerIn,
0023         TECControllerOut:=TECControllerOut, ErrorHandler:=ErrorHandler);
0024
0025 IF TECController.Fault THEN (* Fault = default setting?*)
0026     TECController.TECVoltsOut:=0;
0027     TECController.OldControlSig := 0;
0028 END_IF;
0029
0030 PIServo(TECController:=TECController, TECControllerIn:=TECControllerIn, (*actual temperature modulation execution*)
0031         TECControllerOut:=TECControllerOut, ErrorHandler:=ErrorHandler);
0032
0033 ErrorHandler (ErrorMethod := Init, Error := TECController.Error);
0034                 ,
0035
```

Figure 26: TwinCat PLC Screenshot of the Temperature Servo Code

D More Data from Experiment

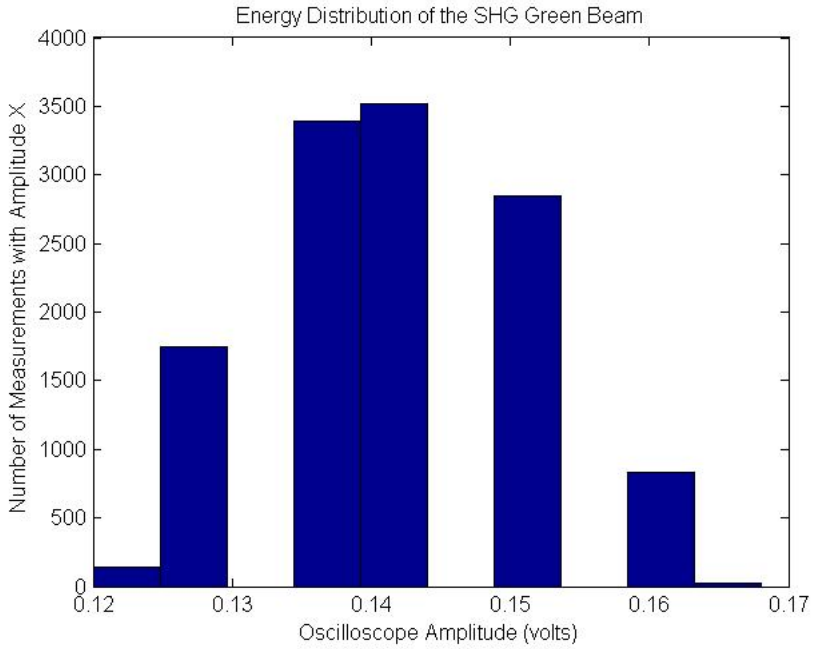

,

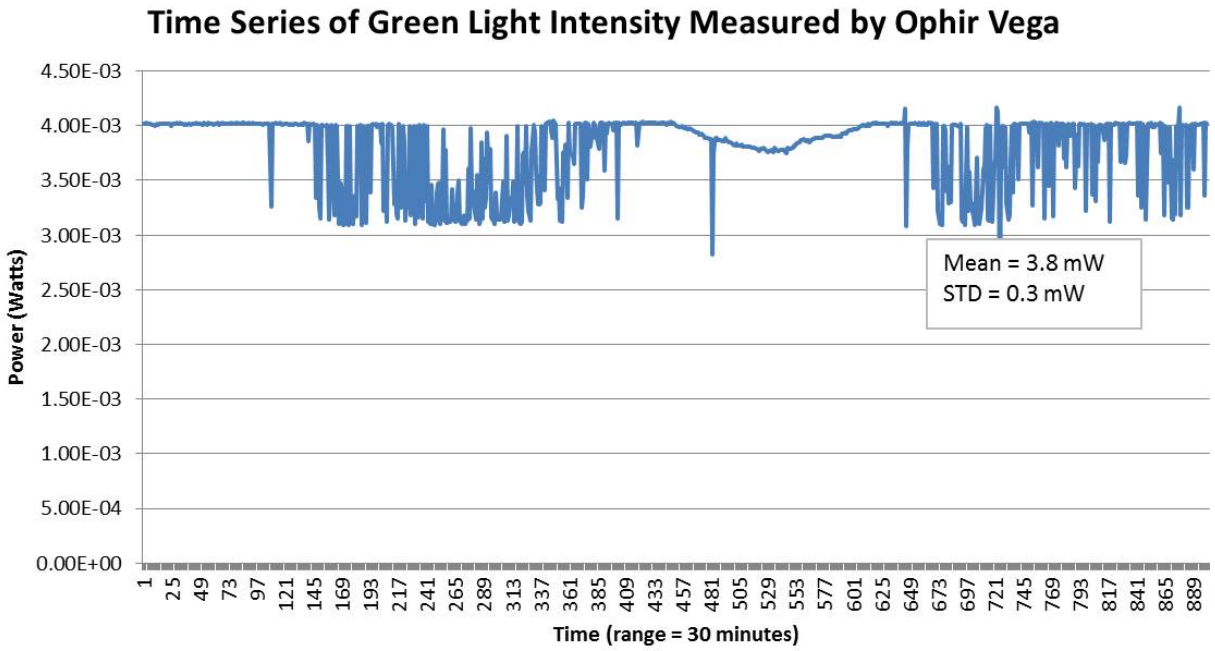

Figure 27: Ophir Time Series of Green Beam Power

,

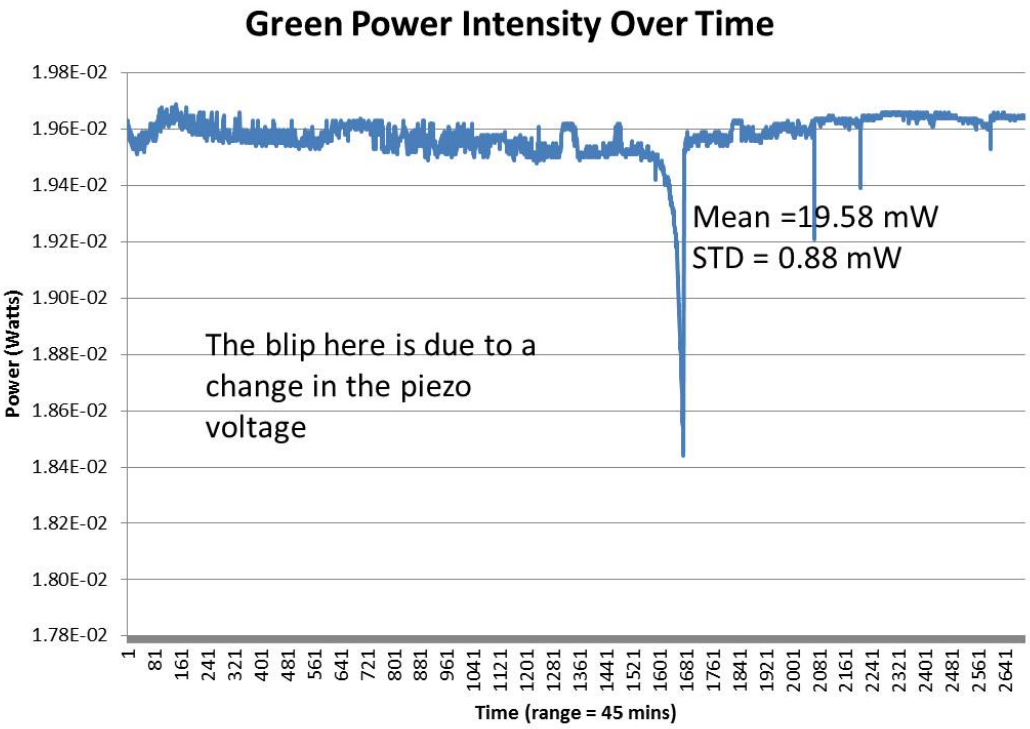
Green Power Intensity Over Time
Power (Watts)
1.98E-02
1.96E-02
1.94E-02
1.92E-02
1.90E-02
1.88E-02
1.86E-02
1.84E-02
1.82E-02
1.80E-02
1.78E-02
Mean =19.58 mW
STD = 0.88 mW
The blip here is due to a change in the piezo voltage
1 81 161 241 321 401 481 561 641 721 801 881 961 1041 1121 1201 1281 1361 1441 1521 1601 1681 1761 1841 1921 2001 2081 2161 2241 2321 2401 2481 2561 2641
Time (range = 45 mins)

,

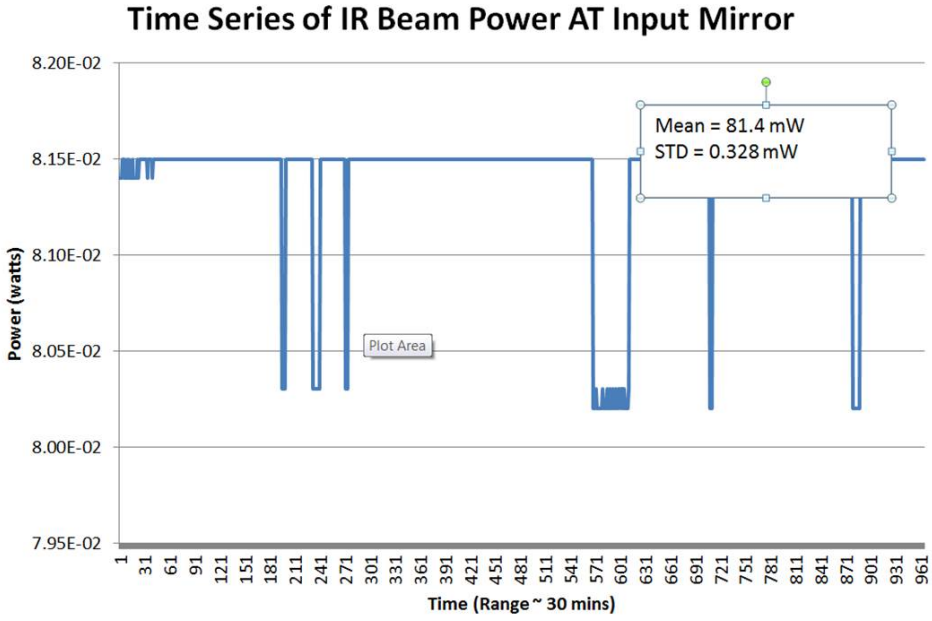
Time Series of IR Beam Power AT Input Mirror
Power (watts)
8.20E-02
8.15E-02
8.10E-02
8.05E-02
8.00E-02
7.95E-02
Mean = 81.4 mW
STD = 0.328 mW
Plot Area
1 31 61 91 121 151 181 211 241 271 301 331 361 391 421 451 481 511 541 571 601 631 661 691 721 751 781 811 841 871 901 931 961
Time (Range ~ 30 mins)

,

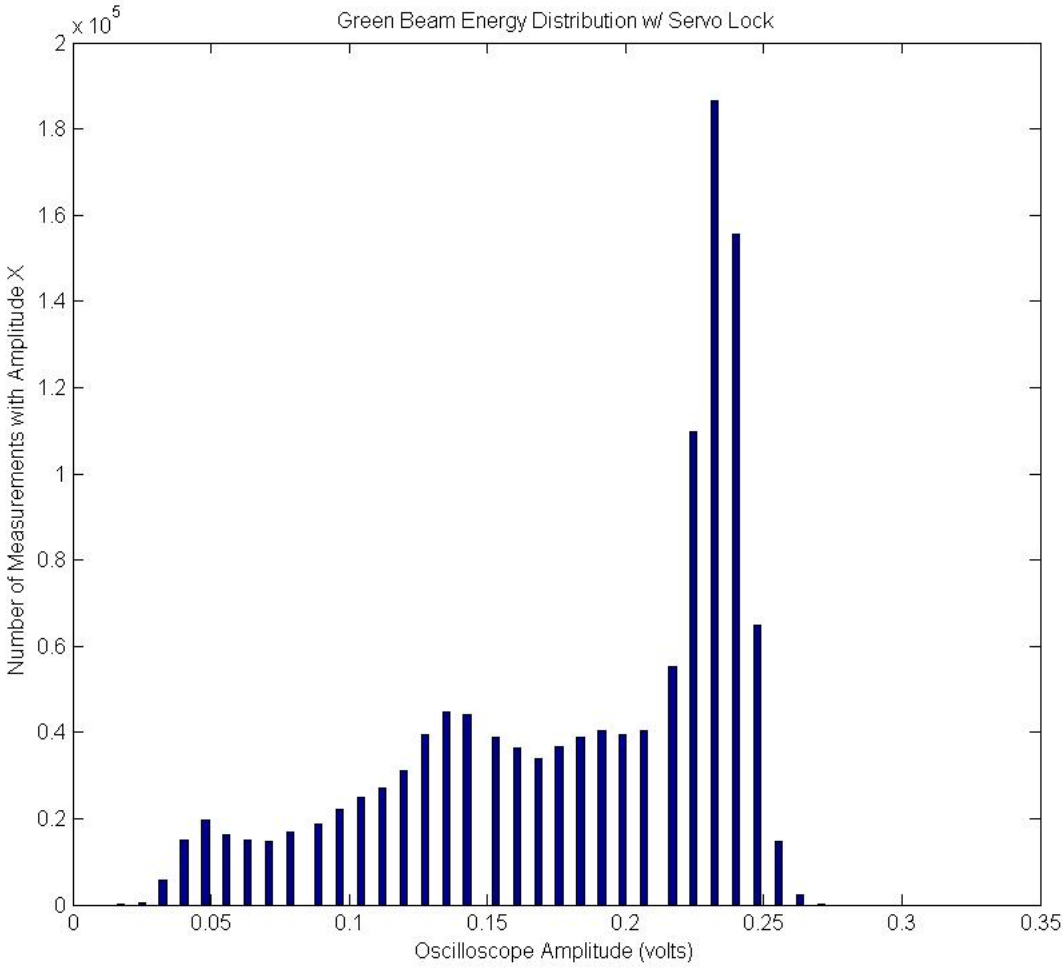

Figure 28: Histogram of Green Beam Energy Distribution Measured by Oscilloscope

References

[1] Erick Black. Notes on pound drever hall technique, 1998. accessed 8/15/2013.

[2] Robert Boyd. *Nonlinear Optics*. Elsevier, Inc., 2008.

[3] Erik Cheever. Unit response, 2013. accessed 8/15/2013.

[4] Michiel Dood. Second harmonic generation. *Huygens Laboratorium*, 2006.

[5] Eugene Hecht. *Optics*. Addison-Wesley Publishing Company, 2001.

[6] Tony F. Heinz Jerry Dadap, Jie Shan. Theory of optical second harmonic generation from a sphere of centrosymmetric material: Small particle limit. *Journal of the American Optical Society B*, 2004.

[7] S. Chaitanya Kumar. High power single frequency continuous frequency single wave second harmonic generation of ytterbium fiber laser in ppktp and mgo:spplt. *Optics Express*, 2009.

[8] Andres Medina. Characterization of second harmonic generators for advanced ligo, August 2013. DCC LIGO.

[9] M Nickerson. An introduction to pound drever hall laser frequency locking. *American Journal of Physics*, 2001.

[10] Rudiger Paschotta. Rp photonics encyclopedia: Frequency doubling, 2013. accessed 8/15/2013.

[11] Rudiger Paschotta. Rp photonics encyclopedia: Noncritical phase matching, 2013. accessed 8/15/2013.

[12] Rudiger Paschotta. Rp photonics encyclopedia: Resonator modes, 2013.